

# R-Parity Violation and Direct Stau Pair Production at the LHC

Herbert K. Dreiner\*

*Bethe Center for Theoretical Physics & Physikalisches Institut der Universität Bonn,  
 Nußallee 12, 53115 Bonn, Germany*

Víctor Martín Lozano†

*Bethe Center for Theoretical Physics & Physikalisches Institut der Universität Bonn,  
 Nußallee 12, 53115 Bonn, Germany,  
 and DESY, Notkestraße 85, 22607 Hamburg, Germany*

We consider pair production of LSP staus at the LHC within R-parity violating supersymmetry. The staus decay into Standard Model leptons through the  $LL\bar{E}$  operator. Using `CheckMATE` we have recast multileptonic searches to test such scenarios. We show for the first time that using these analyses the stau mass can be constrained up to 345 GeV, depending on the stau decay mode, as well as the stau mixing angle. However, there is for all scenarios a significant gap between the lower LEP limit on the stau mass and the onset of the LHC sensitivity. This approach can be used in the future to constrain the stau sector in the context of RPV lepton-number violating models.

## I. INTRODUCTION

Supersymmetry [1, 2] is a widely considered possible solution to the hierarchy problem [3, 4]. When extending the Poincaré and gauge symmetries of the Standard Model of particle physics (SM) to include supersymmetry, in the minimal version, the particle content must be doubled, matching fermions with bosons. Furthermore an extra Higgs doublet is added. The most general renormalizable superpotential with this field content is

$$W_{\text{SSM}} = W_{\text{MSSM}} + W_{\text{RPV}}, \quad (1)$$

$$W_{\text{MSSM}} = \epsilon_{ab} [h_{ij}^E L_i^a H_d^b \bar{E}_j + h_{ij}^D Q_i^a H_d^b \bar{D}_j + h_{ij}^U Q_i^a H_u^b \bar{U}_j + \mu H_d^a H_u^b], \quad (2)$$

$$W_{\text{RPV}} = \epsilon_{ab} \left[ \frac{1}{2} \lambda_{ijk} L_i^a L_j^b \bar{E}_k + \lambda'_{ijk} L_i^a Q_j^b \bar{D}_k - \kappa_i L_i^a H_u^b \right] + \frac{1}{2} \epsilon_{xyz} \lambda''_{ijk} \bar{U}_i^x \bar{D}_j^y \bar{D}_k^z. \quad (3)$$

Here we have used the common notation employing chiral superfields of for example Ref. [5, 6]. The operators in Eq. (2) lead to masses for the SM fermions and mixing in the Higgs sector. The operators in the first line of Eq. (3) violate lepton-number, those in the second line violate baryon-number. Together these latter operators lead to a proton decay rate in disagreement with the experimental limits, unless the couplings are extremely small, see for example Ref. [7]. In the case of the MSSM (minimal supersymmetric Standard Model) the discrete multiplicative symmetry R-parity is imposed, where

$$R_p = (-1)^{2S+3B+L}, \quad (4)$$

with  $S$  the spin,  $B$  the baryon-number and  $L$  the lepton-number of a particle [8]. This prohibits all the baryon- and lepton-number violating operators in Eq. (3) and the proton is stable. Furthermore, in such R-parity conserving supersymmetric models (RPC) the lightest supersymmetric particle (LSP) is stable. For cosmological reasons it must be electrically neutral [9] and is usually considered to be the lightest neutralino. It has been extensively studied as a dark matter candidate [10]. The RPC model must be extended for example by a heavy see-saw sector to allow for light neutrino masses. R-parity is discrete gauge anomaly-free [11], however it allows for dimension-five proton decay operators. Thus the symmetry proton hexality  $P_6$ , is preferable, which at colliders is phenomenologically equivalent [12].

Models where a subset of the terms in Eq. (3) are allowed are called R-parity violating supersymmetric models, short RPV models [6, 13, 14]. For example with the discrete symmetry baryon triality [15, 16] only the lepton-number violating couplings are allowed. Just as R-parity, baryon triality is discrete gauge anomaly-free [11, 12, 17], and can thus be consistently embedded in higher energy models without violation through quantum gravity effects. From a theoretical point of view RPV models are thus at least as well motivated as R-parity conserving models. As a benefit, light neutrino masses are obtained automatically [15, 16, 18, 19], notably *without* an additional heavy Majorana neutrino scale.

Due to the terms in  $W_{\text{RPV}}$  the neutralino LSP is no longer stable and is not a dark matter candidate. Instead, a potential dark matter candidate is the axino [20–23], which is also unstable, but due to the small coupling is long lived on cosmological time scales. We shall not further consider the axino here as it is irrelevant for collider physics. We denote as the LSP, the lightest non-axino supersymmetric particle.

Since the LSP is not constrained by cosmological

\* dreiner@uni-bonn.de

† victor.lozano@desy.de

considerations, in principle any supersymmetric particle (sparticle) can be the LSP. Allowing for any sparticle to be the LSP leads to a very wide range of potential signatures at the LHC, many dramatically different from the standard missing transverse momentum signatures in RPC [24–26]. If we assume a simple set of boundary conditions for the supersymmetric parameters at the unification scale  $M_X = \mathcal{O}(10^{16} \text{ GeV})$ , *i.e.* the constrained minimal supersymmetric Standard Model (CMSSM) [2, 27, 28] modified by an additional RPV operator, and run the spectrum down to the weak scale via the renormalization group equations (RGEs), including the RPV couplings [5, 6, 25], then only a small set of sparticles can be realized as the LSP [26, 29]. Already in the R-parity conserving CMSSM the stau is the LSP in large regions of parameter space, namely when  $M_0 \lesssim M_{1/2}/6$  [25, 29]. As mentioned, these are excluded for cosmological reasons in RPC [9], however in RPV models they are allowed. Thus even for very small RPV-couplings the stau can be the LSP. These parameter ranges are extended in  $M_0, M_{1/2}$  for larger values of RPV-couplings involving the stau, in particular the right-handed stau, *i.e.*  $\lambda_{ij3}$ , see Fig. 2 in Ref. [26].

In Ref. [26] the coverage of the RPV CMSSM with a stau LSP through existing LHC data was investigated, and found to be almost non-existent [30, 31]. A specific stau-LSP benchmark point is given in Ref. [25]. See also the section on supersymmetric particle searches in the PDG [32]. It is the purpose of this paper to investigate the phenomenology of supersymmetric RPV stau-LSP models at the LHC. To be definite, we focus on solely non-zero  $LL\bar{E}$  operators, for which the stau decays directly via a two-body mode, *i.e.*  $L_i L_j \bar{E}_3$ , or  $L_i L_3 \bar{E}_{1,2}$ , with  $i, j \in \{1, 2, 3\}$ . The outline of this paper is as follows. In Sec. II we present our model, as well as the specific representative scenarios with their LHC signatures, which we investigate in detail. In Sec. III we discuss the stau decay branching ratios as well as the stau lifetime. In Sec. IV we review the RPV stau searches at LEP, in particular the resulting lower mass bounds. In Sec. V we discuss the experimental LHC analyses we employ in recasting. In Sec. VI we present our numerical results and in Sec. VII we offer our conclusions.

## II. MODEL

In the minimal supersymmetric Standard Model, the off-diagonal elements in the left-right (LR) single flavor fermion mass matrices are proportional to the fermion mass. Thus for sleptons, the stau will have the largest mixing. After diagonalizing the mass matrix (see for example Ref. [33]), we obtain the mass eigenstates  $\tilde{\tau}_{1,2}$  in terms of the  $SU(2)_L$  current eigenstates  $\tilde{\tau}_{L,R}$

$$\begin{pmatrix} \tilde{\tau}_1 \\ \tilde{\tau}_2 \end{pmatrix} = \begin{pmatrix} \cos \theta_{\tilde{\tau}} & \sin \theta_{\tilde{\tau}} \\ -\sin \theta_{\tilde{\tau}} & \cos \theta_{\tilde{\tau}} \end{pmatrix} \begin{pmatrix} \tilde{\tau}_L \\ \tilde{\tau}_R \end{pmatrix}. \quad (5)$$

Model	Coupling	$\tilde{\tau}_1$ -Decays	Signatures
Ia	$\lambda_{a31}$	$e\nu_a$	$e^+e^- + \cancel{E}_T$
Ib	$\lambda_{a32}$	$\mu\nu_a$	$\mu^+\mu^- + \cancel{E}_T$
II	$\lambda_{123}$	$\mu\nu_e, e\nu_\mu$	$e^+e^- + \cancel{E}_T$ $\mu^+\mu^- + \cancel{E}_T$ $e^\pm\mu^\mp + \cancel{E}_T$
IIIa	$\lambda_{133}$	$e\nu_\tau, \tau\nu_e$	$e^+e^- + \cancel{E}_T$ $\tau^+\tau^- + \cancel{E}_T$ $e^\pm\tau^\mp + \cancel{E}_T$
IIIb	$\lambda_{233}$	$\mu\nu_\tau, \tau\nu_\mu$	$\mu^+\mu^- + \cancel{E}_T$ $\tau^+\tau^- + \cancel{E}_T$ $\mu^\pm\tau^\mp + \cancel{E}_T$

TABLE I. Signatures for the pair production of staus at the LHC, with two-body decays of the staus via the  $LL\bar{E}$  operators. Column 2 lists the dominant single coupling we consider, column and in particular those leading to two-body decays of the staus, column 2. This leads to five models, when considering  $e^\pm$  and  $\mu^\pm$  separately, column 1. In column 3 we list the decay modes of the  $\tilde{\tau}_1$  and in column 4 the signatures for a pair of staus. Here the generation index  $a = 1, 2$ .

Here for the masses:  $m_{\tilde{\tau}_1} < m_{\tilde{\tau}_2}$ , and  $\theta_{\tilde{\tau}}$  is the mixing angle in the stau sector. Together with the stau mass it is the main free parameter in our analysis. For  $\theta_{\tilde{\tau}} = 0$  the lightest stau,  $\tilde{\tau}_1$ , is pure  $\tilde{\tau}_L$ , for  $\theta_{\tilde{\tau}} = \frac{\pi}{2}$  it is pure  $\tilde{\tau}_R$ . In the following we consider the lightest stau to be the LSP and analyze direct pair production at the LHC

$$pp \rightarrow \tilde{\tau}_1^+ \tilde{\tau}_1^- + X. \quad (6)$$

Here we only consider the production of the staus via gauge couplings, *i.e.* we consider the RPV couplings to be small compared to the gauge couplings, in accordance with the present limits [14, 34, 35]. (For larger couplings single sparticle production is more promising [36–38].) R-parity violation leads to the stau decaying in the detector, if the RPV coupling is not too small. We discuss this in detail below. Depending on the decay mode, we focus on three different models, each with only one dominant RPV operator, and for which the stau decays as

$$\text{Model I: } L_a L_3 \bar{E}_c, \quad \tilde{\tau}_1^+ \rightarrow \ell_c^+ \nu_a, \quad (7)$$

$$\text{Model II: } L_1 L_2 \bar{E}_3, \quad \tilde{\tau}_1^+ \rightarrow (e^+ \bar{\nu}_\mu, \mu^+ \bar{\nu}_e), \quad (8)$$

$$\text{Model III: } L_a L_3 \bar{E}_3, \quad \tilde{\tau}_1^+ \rightarrow (\tau^+ \nu_a, \tau^+ \bar{\nu}_a, \ell_a^+ \nu_\tau), \quad (9)$$

where  $a, c \in \{1, 2\}$ , and the  $\tilde{\tau}_1^-$  decay to the charge conjugate final states.

Out of Models I-III in Eqs. (7)-(9), we consider 5 separate scenarios, which are listed in Tab. I. We consider Model I with  $c = 1$  as Model Ia, and with  $c = 2$  as Model Ib. Similarly we shall consider Model III separately with  $a = 1$ , Model IIIa, and with  $a = 2$ , Model IIIb. This corresponds to treating electrons and muons separately.

Below we discuss each scenario in detail. We recast them in terms of LHC searches implemented in the pro-

gram CheckMATE [39, 40]. As we see below, the most relevant searches are the ones with leptons and missing energy in the final state, which are dedicated to the search for electroweakinos or stop squarks.

### III. STAU DECAYS

#### A. Branching Ratios

According to Eq. (5), the lightest stau eigenstate is given by the mixture

$$\tilde{\tau}_1 = \cos \theta_{\tilde{\tau}} \tilde{\tau}_L + \sin \theta_{\tilde{\tau}} \cdot \tilde{\tau}_R. \quad (10)$$

In Model I only the  $\tilde{\tau}_L$ -component of  $\tilde{\tau}_1$  couples to the dominant operator. Furthermore there is only one two-body decay mode. In this case the  $\tilde{\tau}_1$  decay rate is given by [41]

$$\Gamma(\tilde{\tau}_1^+ \rightarrow \ell_c^+ \nu_a) = |\lambda_{a3c}|^2 \cos^2 \theta_{\tilde{\tau}} \frac{(m_{\tilde{\tau}_1}^2 - m_{\ell_c}^2)^2}{16\pi m_{\tilde{\tau}_1}^3}, \quad (11)$$

where  $\ell_c^+$  denotes the final state charged lepton of generation  $c = 1, 2$ , and  $m_{\ell_c}$  its mass. For  $\theta_{\tilde{\tau}} \rightarrow \frac{\pi}{2}$  this decay width vanishes. The stau then decays to a four-body final state [6, 25] via a virtual neutralino

$$\tilde{\tau}_1^- \rightarrow \tau^- + (\tilde{\chi}_1^0)^* \rightarrow \tau^- + (\tau^\pm \ell_c^\mp \nu_a, \ell_a^\pm \ell_c^\mp \nu_\tau), \quad (12)$$

with a total of four decay modes. The decay rate is given in the appendix of Ref. [6]. For fixed slepton and neutralino mass the partial width goes as  $m_{\tilde{\tau}_1}^7$ . A related decay via the chargino is also possible,

$$\tilde{\tau}_1^- \rightarrow \nu_\tau + (\tilde{\chi}_1^-)^* \rightarrow \nu_\tau + (\ell_a^\pm \tau^\mp \ell_c^\mp, \nu_a \nu_\tau \ell_c^-), \quad (13)$$

with a similar decay rate. We have assumed here that the lightest chargino is wino dominated.

In Fig. 1 we show isocurves of  $R \equiv \Gamma_{4\text{-body}}/\Gamma_{2\text{-body}}$ , the ratio of the four-body stau decay width over the two-body decay width as a function of the stau mass,  $m_{\tilde{\tau}_1}$ , and  $\cos \theta_{\tilde{\tau}}$  for intermediate masses of  $m_{\tilde{\chi}} = m_{\tilde{\ell}} = 500$  GeV. These intermediate masses are chosen to maximize the four-body partial decay width. For the neutralino for simplicity, we have assumed  $SU(2)_L$  couplings only. The ratio  $R$  grows with  $m_{\tilde{\tau}_1}$  as expected, but remains smaller than about  $10^{-3}$  except for the mixing angle very close to  $\pi/2$ . Thus for most of the parameter region the two-body decays are sufficient to understand the results. However, we include the four-body decays in our complete analysis.

In Model II, it is only the  $\tilde{\tau}_R$ -component of  $\tilde{\tau}_1$  which couples directly to the RPV operator, and there are two decay modes. One partial decay width is given by

$$\Gamma(\tilde{\tau}_1^+ \rightarrow e^+ \bar{\nu}_\mu) = |\lambda_{123}|^2 \sin^2 \theta_{\tilde{\tau}} \frac{(m_{\tilde{\tau}_1}^2 - m_e^2)^2}{16\pi m_{\tilde{\tau}_1}^3}. \quad (14)$$

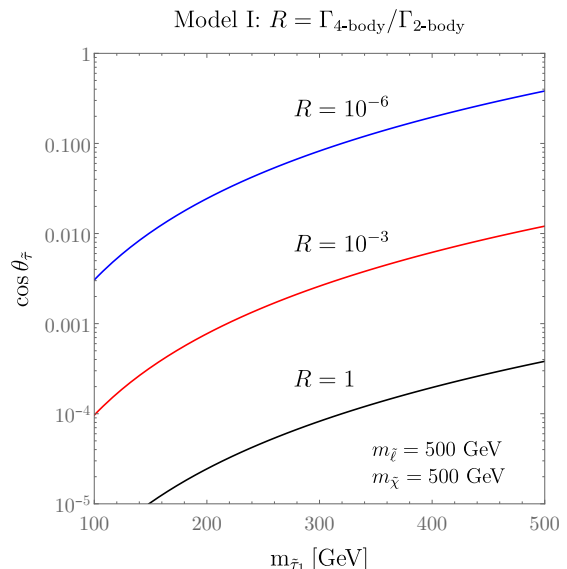


FIG. 1. Isocurves of the ratio of the four-body and the two-body stau decay widths as a function of the stau mass and  $\cos \theta_{\tilde{\tau}}$  in Model I for masses of the intermediate particles  $m_{\tilde{\chi}} = m_{\tilde{\ell}} = 500$  GeV. For the neutralino for simplicity, we have assumed  $SU(2)_L$  couplings only.

For the other decay rate,  $\Gamma(\tilde{\tau}_1 \rightarrow \mu^+ \bar{\nu}_e)$ , replace  $m_e \rightarrow m_\mu$ . Neglecting the electron and muon masses, the rates for these two decays in Model II are equal. The branching ratios are 50%, respectively, if there are no further decay modes. For  $\theta_{\tilde{\tau}} \rightarrow 0$  the decay rate vanishes and the corresponding four-body decay modes via virtual electroweakinos must be included. In Fig. 2 we plot isocurves of the ratio  $R$  as a function  $m_{\tilde{\tau}_1}$  and  $\sin \theta_{\tilde{\tau}}$ . In this model  $R > 0.01$  for  $\theta_{\tilde{\tau}} > 5 \cdot 10^{-3}$ , and the four-body decays can mostly be neglected.

In Model III, both the  $\tilde{\tau}_R$  and the  $\tilde{\tau}_L$  components separately couple to the dominant operator. The partial widths for the three decay modes are

$$\Gamma(\tilde{\tau}_1^+ \rightarrow \tau^+ \bar{\nu}_a) = |\lambda_{a33}|^2 \sin^2 \theta_{\tilde{\tau}} \frac{(m_{\tilde{\tau}_1}^2 - m_\tau^2)^2}{16\pi m_{\tilde{\tau}_1}^3}, \quad (15)$$

$$\Gamma(\tilde{\tau}_1^+ \rightarrow \ell_a^+ \bar{\nu}_3) = |\lambda_{a33}|^2 \sin^2 \theta_{\tilde{\tau}} \frac{(m_{\tilde{\tau}_1}^2 - m_{\ell_a}^2)^2}{16\pi m_{\tilde{\tau}_1}^3}, \quad (16)$$

$$\Gamma(\tilde{\tau}_1^+ \rightarrow \tau^+ \nu_a) = |\lambda_{a33}|^2 \cos^2 \theta_{\tilde{\tau}} \frac{(m_{\tilde{\tau}_1}^2 - m_\tau^2)^2}{16\pi m_{\tilde{\tau}_1}^3}. \quad (17)$$

Neglecting the final-state charged lepton masses compared to the stau mass we thus have for the total width

$$\Gamma(\tilde{\tau}_1^+ \rightarrow \tau^+ \nu_a) = \frac{|\lambda_{a33}|^2}{16\pi} (1 + \sin^2 \theta_{\tilde{\tau}}) m_{\tilde{\tau}_1}, \quad (18)$$

which is non-zero for all values of the stau mixing angle. Therefore  $R \ll 1$  over the entire parameter range we consider here, as can be seen in Fig. 3.

Assuming that only the two-body decays are dominant and combining the two decays to  $\tau^+$ 's, Eqs. (15) and (17),

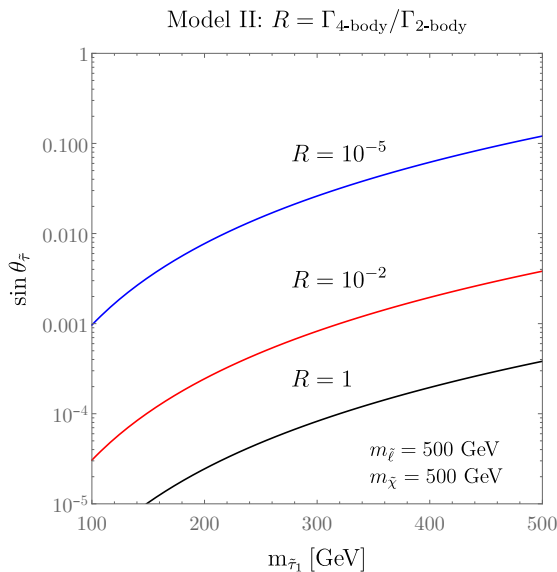


FIG. 2. Isocurves of the ratio of the two-body and the two-body stau decay widths as a function of the stau mass and  $\cos \theta_{\tilde{\tau}}$  in Model II for masses of the intermediate particles  $m_{\tilde{\chi}} = m_{\tilde{\ell}} = 500$  GeV.

which are observationally equivalent, we obtain for the pure two-body branching ratios

$$\text{Br}(\tilde{\tau}_1 \rightarrow \{\tau^+ \bar{\nu}_a, \tau^+ \nu_e\}) = \frac{1}{1 + \sin^2 \theta_{\tilde{\tau}}}, \quad (19)$$

$$\text{Br}(\tilde{\tau}_1 \rightarrow \ell_a^+ \bar{\nu}_{\tilde{\tau}}) = \frac{\sin^2 \theta_{\tilde{\tau}}}{1 + \sin^2 \theta_{\tilde{\tau}}}. \quad (20)$$

Thus for  $\cos \theta_{\tilde{\tau}} \rightarrow 1$  the stau decays 100% to  $\tau$ -leptons, which is important for searches. The maximum branching ratio to  $\ell_a^+ \in \{e^+, \mu^+\}$  is only 50%, obtained for  $\cos \theta_{\tilde{\tau}} \rightarrow 0$ .

### B. Stau Decay length

We next consider an estimate for the stau LSP lifetime. Ignoring the final state charged lepton masses, using only the two-body decay width formula, and setting  $m_{\tilde{\tau}_1} = 250$  GeV we estimate

$$\tau_{\tilde{\tau}_1} = \frac{1.3 \cdot 10^{-25} \text{ s}}{\lambda_{ijk}^2 \cdot A_{\theta_{\tilde{\tau}}}^2} \quad (21)$$

where  $A_{\theta_{\tilde{\tau}}}^2 \equiv [\text{I: } \cos^2 \theta_{\tilde{\tau}}; \text{II: } \sin^2 \theta_{\tilde{\tau}}; \text{III: } (1 + \sin^2 \theta_{\tilde{\tau}})]$ . Thus for

$$\lambda_{ijk} \cdot A_{\theta_{\tilde{\tau}}} \gtrsim 2 \cdot 10^{-7} \quad (22)$$

the stau decays promptly in the detector,  $c\tau_{\tilde{\tau}_1} \lesssim 1$  mm. Depending on the stau mixing angle, for a wide range of couplings,  $\lambda_{ijk}$ , consistent with existing upper bounds

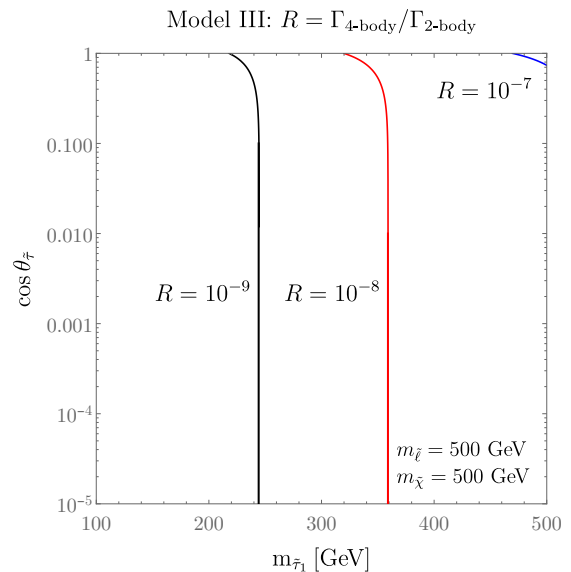


FIG. 3. Isocurves of the ratio of the four-body and the two-body stau decay widths as a function of the stau mass and  $\cos \theta_{\tilde{\tau}}$  in Model III for masses of the intermediate particles  $m_{\tilde{\chi}} = m_{\tilde{\ell}} = 500$  GeV.

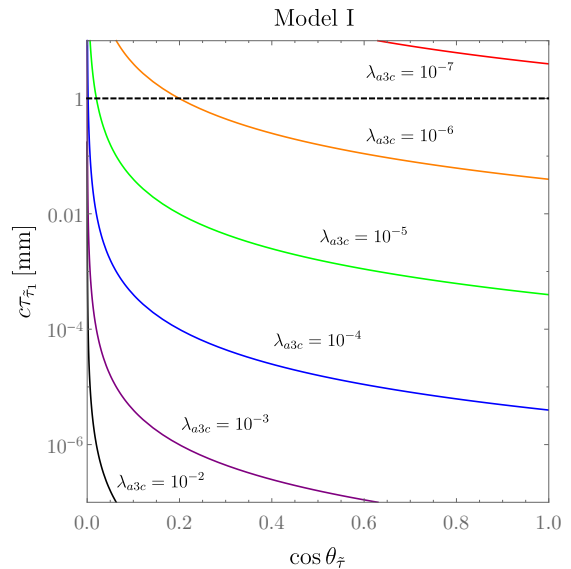


FIG. 4. Decay length of the stau LSP,  $\tilde{\tau}_1$ , as a function of the mixing angle,  $\cos \theta_{\tilde{\tau}}$ , for different values of the  $\lambda_{a3c}$  coupling.

[14, 34, 42–44], we can consider the staus to decay promptly.<sup>1</sup>

We performed the complete computation to check

<sup>1</sup> In related recent work [45] on RPV tau physics at the LHC, bounds were set on the  $\lambda'$  couplings in  $LQ\bar{D}$  scenarios, which we shall discuss elsewhere.

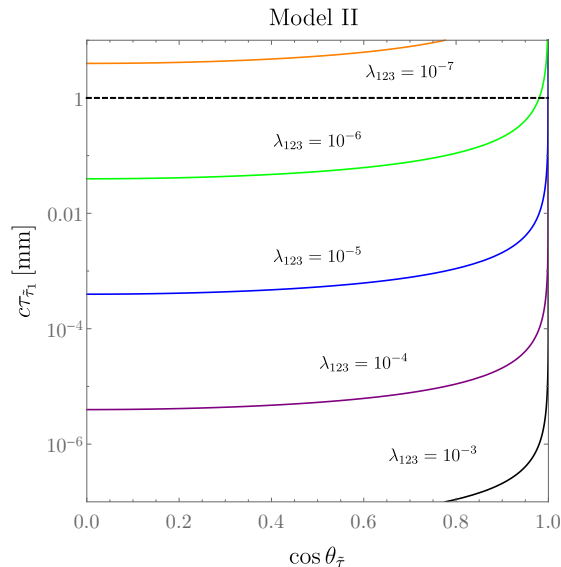


FIG. 5. Decay length of the stau LSP,  $\tilde{\tau}_1$ , as a function of the mixing angle,  $\cos \theta_{\tilde{\tau}}$ , for different values of the  $\lambda_{123}$  coupling.

Eq. (22) quantitatively. In Fig. 4 we plot the decay length for  $m_{\tilde{\tau}_1} = 250$  GeV, as a function of the mixing angle,  $\cos \theta_{\tilde{\tau}}$ , for different values of the coupling  $\lambda_{a3c}$ , *i.e.* Model I. The horizontal dashed line denotes  $c\tau_{\tilde{\tau}_1} = 1$  mm, below which we consider the decay prompt. When the mixing angle approaches  $\pi/2$ , *i.e.*  $\cos \theta_{\tilde{\tau}} \rightarrow 0$ , the decay length grows, as expected from Eq. (11), but then the four-body decays kick in. In this extreme case the stau becomes long-lived for  $\lambda_{a3c} \lesssim 3 \cdot 10^{-7}$ . For  $\lambda_{a3c} \lesssim 10^{-5}$  the stau becomes long-lived for non-negligible values of  $\cos \theta_{\tilde{\tau}}$ . In particular, for  $\lambda_{a3c} = 10^{-6}$ , we have  $c\tau_{\tilde{\tau}_1} > 1$  mm for  $\cos \theta_{\tilde{\tau}} < 0.174$ . For  $\lambda_{a3c} < 3 \cdot 10^{-7}$ , we find  $c\tau \geq 1$  mm independently of the mixing angle.

In Model II we show in Fig. 5 the stau decay length as a function of the mixing angle,  $\cos \theta_{\tilde{\tau}}$ , for different values of the parameter  $\lambda_{123}$ . Unlike Model I, the stau becomes long-lived for mixing angles close to 0 ( $\cos \theta_{\tilde{\tau}} \rightarrow 1$ ), *cf.* Eq. (14). For  $\lambda_{123} \lesssim 1.5 \cdot 10^{-7}$  the decay length becomes greater than  $c\tau \geq 1$  mm, basically for all mixing angles.

The analogous plot for Model III is shown in Fig. 6. Here the decay length is practically independent of the mixing angle. There is only a moderate increase for  $\cos \theta_{\tilde{\tau}} \rightarrow 1$ . This is expected from Eq. (18), due to the term independent of  $\theta_{\tilde{\tau}}$ . The decay is prompt for  $\lambda_{a33} \gtrsim 1.5 \cdot 10^{-7}$ , for all  $\theta_{\tilde{\tau}}$ .

We therefore assume that in every model the parameter  $\lambda_{ijk}$  is such that the stau decays promptly. As we have seen in Figs. 4, 5 and 6 one can assure that this condition is fulfilled when  $\lambda_{ijk} \gtrsim 10^{-6}$ .

For  $m_{\tilde{\tau}_1} \gtrsim 150$  GeV the low-energy constraints on the R-parity violating couplings are fulfilled for  $\lambda_{ijk} < 0.1$  [26, 43], which is beyond the range plotted in Figs. 4, 5 and 6.

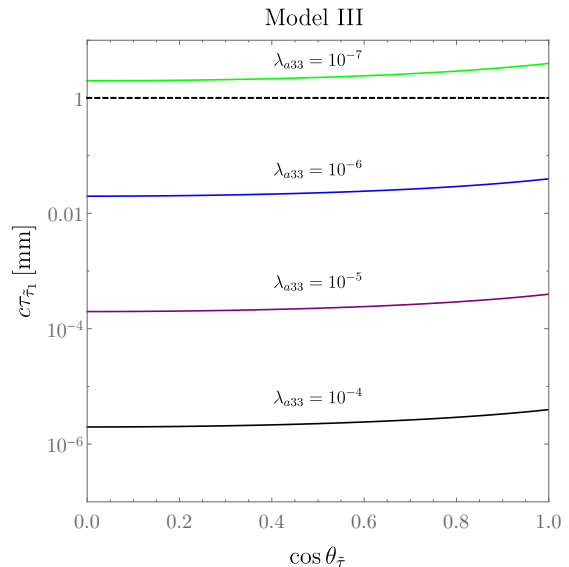


FIG. 6. Decay length of the stau LSP,  $\tilde{\tau}_1$ , as a function of the mixing angle,  $\cos \theta_{\tilde{\tau}}$ , for different values of the  $\lambda_{a33}$  coupling.

#### IV. LOWER LEP LIMITS ON STAU MASS

All four experiments at LEP have published papers on searches for staus in RPV supersymmetric scenarios; ALEPH: [46], DELPHI [47], L3 [48], and OPAL [49]. We briefly summarize their results here, as we need them below. The experiments do not perform a systematic analysis of the bounds for a stau LSP for arbitrary mixing angles, which is what we would need. Most of the analyses are on pure right-handed staus, since in unification scale models the largest component of  $\tilde{\tau}_1$  is typically  $\tilde{\tau}_R$ , with a few mass searches also for pure  $\tilde{\tau}_L$ . We thus consider the lower mass bounds at the limiting cases of mixing, *i.e.* for  $\cos \theta_{\tilde{\tau}} = 0$  and  $\cos \theta_{\tilde{\tau}} = 1$  and interpolate these for our results in Figs. 7-10, below.

All experiments consider direct two-body decays of the staus via the  $LL\bar{E}$  operators, as well as indirect decays via an intermediate neutralino, *i.e.* the chargino decays are mentioned, but not taken into account. Both cases are treated separately with 100% branching ratio, respectively, *i.e.* either with 100% two-body decays, or 100% four-body decays. In the indirect case, the neutralino is assumed to be on-shell, and thus lighter than the stau. This does not correspond to our scenarios. We consider these searches all the same as constraints on our models, as we believe the essential feature is the kinematics of the four-body decay of the stau. This is underlined by the fact, that the bounds depend only weakly on the neutralino mass outside the kinematic boundaries. We then employ the following bounds at the limiting values.

**Models Ia,b:** for  $\cos \theta = 0$  we use the DELPHI and OPAL limits on indirect decays of a  $\tilde{\tau}_R$ :  $m_{\tilde{\tau}_R} > 92$  GeV. For  $\cos \theta = 1$ , OPAL have a limit on direct decays of  $\tilde{\tau}_L$ :

$m_{\tilde{\tau}_R} > 74$  GeV, which we employ.

**Models II:** for  $\cos\theta = 0$  we use the ALEPH lower mass limit for direct decays of the stau  $m_{\tilde{\tau}_R} > 87$  GeV. There is no limit on the indirect decay of a pure  $\tilde{\tau}_L$ . Since the production cross section for  $\tilde{\tau}_L$  is higher than for  $\tilde{\tau}_R$  we employ the  $\tilde{\tau}_R$  bound, from the previous case in the hope that this conservative:  $m_{\tilde{\tau}_R} > 92$  GeV.

**Model IIIa:** for this model in both limiting cases,  $\cos\theta_{\tilde{\tau}} = 0$  or 1, we have possible two-body direct decays. Thus in both cases we use the direct limits:  $m_{\tilde{\tau}_R} > 92$  GeV,  $m_{\tilde{\tau}_L} > 74$  GeV.

The red regions in Figs. 7-10, below, are the interpolation of these bounds. We encourage the experiments to go back and reanalyze the LEP data in lieu of the models we consider here.

## V. RECASTING

We now wish to compare the predictions of the models discussed in the previous section to LHC data. For this we recast the simulated model results in terms of existing LHC analyses. In order to study every scenario we have produced benchmark points making use of the spectrum generator SPheno 4.0.0 [50–52]. For each of these points we have generated  $2 \cdot 10^5$  Monte Carlo (MC) events with the event generator Pythia8.219 [53], using the default parton distribution function NNPDF 2.3 [54]. Then we confront the MC events against CheckMATE 2.0.26 [39, 40] which is based on the fast detector simulation Delphes 3.4.0 [55] and the jet reconstruction tool Fastjet 3.2.1 [56, 57]. CheckMATE is an analysis tool designed to test models against several ATLAS and CMS searches at 8 and 13 TeV. In order to obtain more realistic results we apply some correction factors to the leading order cross section calculated by Pythia8. For that purpose we use the NLO stau production cross section given in Ref. [58] for the case of events produced at  $\sqrt{s} = 8$  TeV and Ref. [59] for those at  $\sqrt{s} = 13$  TeV.<sup>2</sup>

In our grid scans for every scenario, we cover the stau mixing angle range:  $\cos\theta_{\tilde{\tau}} \in [0 + \epsilon, 1 - \epsilon]$ , with  $\epsilon = 10^{-3}$ , avoiding the long decay length regions. We consider the mass range:  $m_{\tilde{\tau}_1} \in [100, 500]$  GeV. Although we have made use of all the ATLAS and CMS searches in CheckMATE only a few actually constrain our scenarios. They are listed in Table II. As we see, there are three analyses that are important, two from Run 1 and one from Run 2. We briefly discuss what makes them relevant for our scenarios.

<sup>2</sup> In Ref. [60] the production of sleptons at NNLO+NNLL is considered. However, they found only very moderate increases in the total cross sections compared with the NLO + NLL results. Thus we take only the results of the latter.

$\sqrt{s}$	Reference	Final State	$\mathcal{L}[\text{fb}^{-1}]$
8 TeV	1403.4853 [61]	$2\ell + \cancel{E}_T$	20.3
8 TeV	ATLAS-CONF-2013-049 [62]	$2\ell + \cancel{E}_T$	20.3
13 TeV	ATLAS-CONF-2017-039 [63]	$2 - 3\ell + \cancel{E}_T$	36.1

TABLE II. List of the searches included in CheckMATE which are most relevant for our models. The first column refers to the center-of-mass energy, 8 or 13 TeV. The second column is the name of the analysis with the reference. The final state studied in each analysis is shown in the third column, while the fourth indicates the integrated luminosity used in each search, respectively.

**Search for direct stop production decaying into  $2\ell + \cancel{E}_T$**  (arXiv:1403.4853) [61]: This search for stops focuses on leptonic final states, electrons and muons, with opposite charge. The leptons come from the decay of  $W^\pm$  bosons produced in the decay chain of the stop squarks. The two opposite sign  $W$ 's decay independently, resulting in the combinations:  $ee$ ,  $e\mu$  and  $\mu\mu$ . This is important for studying RPV couplings with various flavor indices. This search was performed for a center-of-mass energy of  $\sqrt{s} = 8$  TeV and an integrated luminosity of  $\mathcal{L} = 20.3 \text{ fb}^{-1}$ .

**Search for direct slepton and chargino production decaying into  $2\ell + \cancel{E}_T$**  (ATLAS-CONF-2013-049) [62]: The aim of this search is the detection of chargino or slepton pairs through their subsequent decays into leptons and missing energy. The analysis focuses on a final state with two leptons and  $\cancel{E}_T$ . This search was performed for a center-of-mass energy of  $\sqrt{s} = 8$  TeV and an integrated luminosity of  $\mathcal{L} = 20.3 \text{ fb}^{-1}$ .

**Search for electroweak production of SUSY particles with  $2 - 3\ell + \cancel{E}_T$**  (ATLAS-CONF-2017-039) [63]: This search focuses on the direct production of charginos and neutralinos and their decays into leptons and missing energy. The signature are 2 or 3 leptons in the final state plus missing energy. It was performed for a center-of-mass energy of  $\sqrt{s} = 13$  TeV and an integrated luminosity of  $\mathcal{L} = 36.1 \text{ fb}^{-1}$ .

In order to determine if a point is excluded or not by a search, CheckMATE compares the estimate of the number of signal events with the 95% C.L. observed limit

$$r = \frac{S - 1.96 \cdot \Delta S}{S_{\text{exp}}^{95}}, \quad (23)$$

here  $S$  stands for the number of signal events within CheckMATE,  $\Delta S$  is the uncertainty due to MC errors<sup>3</sup> and  $S_{\text{exp}}^{95}$  is the 95% C.L. limit on signal events imposed by the experiment. A point is excluded if the value of  $r$  is

<sup>3</sup> In our case we assume that the MC uncertainty to the signal events is only statistical, so it is given by  $\Delta S = \sqrt{S}$ .

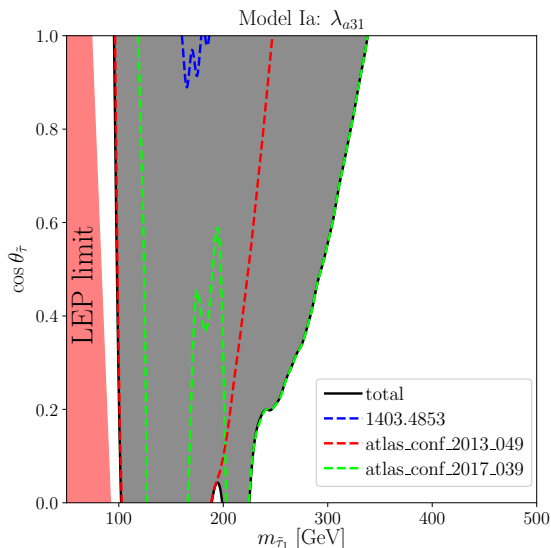


FIG. 7. Exclusion regions for Model Ia as a function of the stau mass and the mixing angle. The different excluded regions due to the different analyses are shown as dashed lines of different colors. The full black line depicts the total exclusion region that is shown as a gray area. The LEP lower stau mass limit in RPV is shown as a red area on the left.

larger than 1.<sup>4</sup>  $r$  is computed for every signal region of every analysis and then the best exclusion limit is chosen, taking the one that presents the best expected exclusion potential. This choice can result in the total exclusion limit being weaker than the limit from a single search in one specific parameter area. Furthermore, **CheckMATE** does not combine searches or signal regions. Thus the limits such determined are conservative.

## VI. NUMERICAL RESULTS

After having defined under which conditions we can consider a model point excluded, we apply these considerations to the different models.

### A. Model Ia

In Model Ia, the relevant operator is  $L_a L_3 \bar{E}_1$ ,  $a = 1, 2$ . As we see in Tab. I, at leading order, the stau decays exclusively as  $\tilde{\tau}^\pm \rightarrow e^\pm \nu_a$ . The final state signature is two opposite sign electrons plus missing energy. The

<sup>4</sup> We do not totally control all the aspects relevant for a true simulation, like systematic errors and higher order corrections. In order to take these uncertainties into account one can define a non-conclusive region defined as the area between  $1.5 > r > 0.67$  where a point cannot be fully allowed or excluded.

results of testing this model against **CheckMATE** are depicted in Fig. 7. The exclusion contours, requiring  $r \geq 1$ , are shown in the  $(m_{\tilde{\tau}_1}, \cos \theta_{\tilde{\tau}})$  plane, as dashed colored curves. The different colors represent the different analyses. The full black line represents the total exclusion limit, which encompasses the gray area.

The blue-dashed line denotes the exclusion from direct stop production followed by leptonic decays at  $\sqrt{s} = 8$  TeV of Ref. [61]. This analysis excludes only a small parameter range around  $m_{\tilde{\tau}_1} = 150 - 180$  GeV and  $\cos \theta_{\tilde{\tau}} > 0.9$ . It has only a weak sensitivity, as it was designed to look for same- and different-flavour final state leptons, while here only electrons are present.

The red-dashed line corresponds to the two-lepton analysis at  $\sqrt{s} = 8$  TeV of Ref. [62]. Overall this analysis is not designed for light staus below about 100 GeV in mass due to the cuts implemented in the search. The power of this search has a mild dependence on the mixing angle, at the upper mass end. This is because right-handed staus have a smaller production cross section than left-handed staus by about a factor of two in this mass range [58, 59]. For pure  $\tilde{\tau}_R$ ,  $\cos \theta_{\tilde{\tau}} = 0$ , the exclusion of this search reaches up to  $m_{\tilde{\tau}_1} > 185$  GeV. The lower mass bound increases as the stau becomes mixed, up to a mass of 240 GeV for a pure  $\tilde{\tau}_L$ .

The green-dashed line corresponds to the 2-3 leptons plus missing energy analysis at 13 TeV and with an integrated luminosity of  $\mathcal{L} = 36.1 \text{fb}^{-1}$  [63]. This analysis has the highest stau mass sensitivity. For  $\cos \theta_{\tilde{\tau}} = 0$  it reaches upto masses of 225 GeV, and for  $\cos \theta_{\tilde{\tau}} = 1$  it extends all the way upto 322 GeV. However, there is a gap in the sensitivity for stau masses between 165 and 200 GeV ranging upto  $\cos \theta_{\tilde{\tau}} = 0.6$ . This is mainly because for these points the observed events in the experiment are fewer than the expected ones, while in the other regions the observed number of events is bigger than the expected one. This range is mostly covered by the analysis [62], the red-dashed curve. Furthermore, the analysis corresponding to the green-dashed curve also fails for stau masses below about 125 GeV since the cuts are too strict to allow for sensitivity to lighter stau masses.

In red we show on the left the lower limit on the stau mass obtained at LEP, as discussed in Sec. IV. There is a significant gap to the LHC sensitivity.

The total exclusion limit, the combination of the excluded regions, is presented as a full black line, with the enclosed area in dark gray. For  $\theta_{\tilde{\tau}} = 0$ , *i.e.* for the lightest stau being pure  $\tilde{\tau}_L$ , we can exclude masses between about 100 GeV and 322 GeV. At  $\theta_{\tilde{\tau}} = \frac{\pi}{2}$  the upper range is reduced to about 225 GeV, with a small search gap just below 200 GeV in mass. There is a significant gap to the LEP bound at low mass, which is larger at  $\cos \theta_{\tilde{\tau}} = 1$ . The LHC sensitivity is higher at  $\theta_{\tilde{\tau}} = 0$ , since the production cross section is higher for pure  $\tilde{\tau}_L$ .

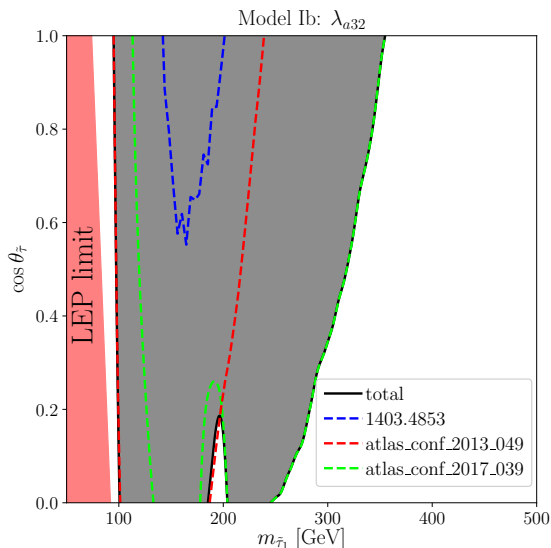


FIG. 8. Exclusion regions for Model Ib as a function of the stau mass and the mixing angle. The code of lines, areas and colors are the same as Fig. 7.

### B. Model Ib

The operator that defines the Model Ib is  $L_a L_3 \bar{E}_2$ ,  $a = 1, 2$ . The principal signature is two opposite sign muons plus missing energy, *cf.* Tab. I. In Fig. 8 we show the results of testing this model against CheckMATE. The same color and line code is used as in Fig. 7. Here the direct stop production search (blue-dashed line) is more sensitive than in the previous case, due to the higher efficiency muon detection. However, this search is not competitive, compared to the other two. The red-dashed line, corresponding to the two-lepton search at 8 TeV, constrains stau masses in the range  $m_{\tilde{\tau}_1} = 100 - 180$  GeV for a mixing angle  $\cos \theta_{\tilde{\tau}} = 0$  and  $m_{\tilde{\tau}_1} = 100 - 245$  GeV for a mixing angle  $\cos \theta_{\tilde{\tau}} = 1$ . The latter is more restrictive, since  $\tilde{\tau}_L$  production is larger than  $\tilde{\tau}_R$ .

The 2-3 lepton search at  $\sqrt{s} = 13$  TeV (green-dashed line) has a better reach in terms of mass exclusion. However, for staus that are mostly right handed,  $\tilde{\tau}_1 \rightarrow \tilde{\tau}_R$ , *i.e.*  $\cos \theta_{\tilde{\tau}} \rightarrow 0$ , the same behaviour as in Model Ia arises, and a small gap just below  $m_{\tilde{\tau}_1} = 200$  GeV appears. Half of this gap is covered by the 2 lepton search at 8 TeV (red-dashed line). As in Model Ia, the 2-3 lepton search at 13 TeV cannot cover well the low mass region due to stricter cuts in the search, and again the 2 lepton search can reach those lower values of the mass. The total exclusion line (solid black) is able to exclude stau masses  $m_{\tilde{\tau}_1} = 100 - 240$  GeV for  $\cos \theta_{\tilde{\tau}} = 0$ , modulo the small gap, and  $m_{\tilde{\tau}_1} = 100 - 345$  GeV for  $\cos \theta_{\tilde{\tau}} = 1$ . Again there is a significant gap between the lower LEP limit, *cf.* Sec. IV, and the low-mass exclusions from the LHC, for all mixing angles.

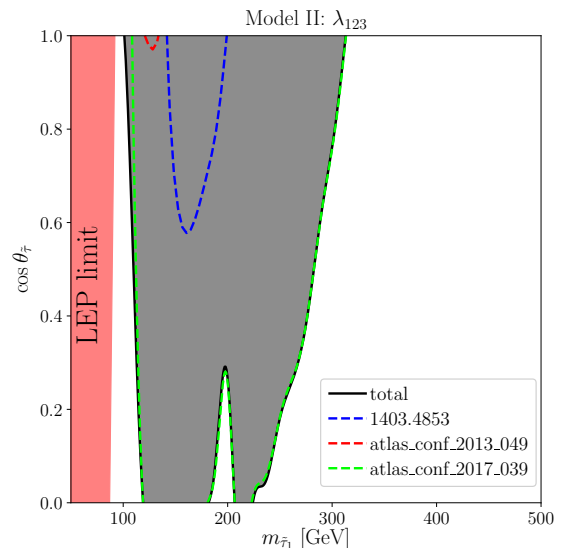


FIG. 9. Exclusion regions for Model II as a function of the stau mass and the mixing angle. The code of lines, areas and colors are the same as Fig. 7.

### C. Model II

The relevant operator for Model II is  $L_1 L_2 \bar{E}_3$ . The stau decay is either  $\tilde{\tau}_1^+ \rightarrow e^+ \bar{\nu}_\mu$  or  $\tilde{\tau}_1^+ \rightarrow \mu^+ \bar{\nu}_e$ , and the final state signatures of stau pair production are  $(e^+ e^- / \mu^+ \mu^- / e^\pm \mu^\mp) + \cancel{E}_T$ . In Fig. 9 the results of testing this model against LHC searches in CheckMATE are shown. The stop pair production search (blue) is now more effective than for Models Ia, Ib. This is due to the inclusion of different flavour lepton signatures. However, it is still not relevant for the final exclusion region. The two lepton search at 8 TeV (red) drops drastically in sensitivity, in comparison with both cases of Model I. One reason is that the different flavours appearing in the final state lower the detectability in this specific search. In this case, as in the previous ones the most powerful in terms of constraining power is the 2-3 lepton search at 13 TeV (green). This search is also coincident with the total exclusion line (black) for this model. Almost pure left-handed staus,  $\cos \theta_{\tilde{\tau}} \rightarrow 1$ , are excluded for the mass range  $m_{\tilde{\tau}_1} = 100 - 305$  GeV, while in the case of right-handed staus,  $\cos \theta_{\tilde{\tau}} \rightarrow 0$ , the excluded mass range is  $m_{\tilde{\tau}_1} = 120 - 180$  GeV and  $m_{\tilde{\tau}_1} = 205 - 225$  GeV. There is also a mass gap in this model between  $m_{\tilde{\tau}_1} = 180 - 205$  GeV. In this case the gap is not partially covered by other searches. Again there is a significant gap at low stau masses above the LEP bound, *cf.* Sec. IV.

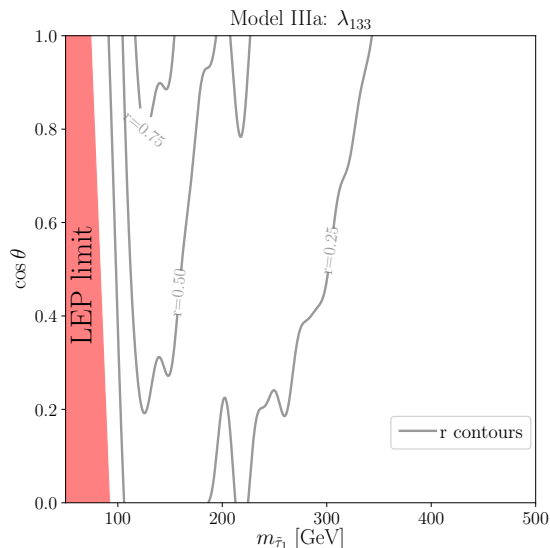


FIG. 10. Recasting of Model IIIa using **CheckMATE**. We show iso-contours of  $r$ , *cf.* Eq. (23), for  $r = 0.25, 0.50$  and  $0.75$ , as a function of the stau mass and the mixing angle.

#### D. Model IIIa

Model IIIa corresponds to the dominant operator  $L_1 L_3 \bar{E}_3$ . The stau decays as  $\tilde{\tau}_1^+ \rightarrow (\tau^+ \nu_e, \tau^+ \bar{\nu}_e, e^+ \nu_\tau)$ , *cf.* Tab. I. The branching ratios are given in Eqs. (19), and (20), as a function of the mixing angle. In Models I and II the staus decay 100% to charged electrons or muons. In Models IIIa and below in IIIb at least 50% of the two-body decays are to  $\tau$ 's, depending on the mixing angle. This significantly degrades the experimental sensitivity, since the implemented searches do not involve  $\tau$ -signatures. In Fig. 10 we show the results of recasting this model in **CheckMATE**, in particular iso-contours of  $r$ , *cf.* Eq. (23). We do not find any region with  $r \geq 1$  and therefore the current searches are not sensitive enough to constrain this model. The most sensitive area,  $r > 0.5$  in the  $(m_{\tilde{\tau}_1}, \cos \theta_{\tilde{\tau}})$  plane is roughly for  $100 \text{ GeV} < m_{\tilde{\tau}_1} < 200 \text{ GeV}$  and  $\cos \theta_{\tilde{\tau}} > 0.25$ . This results mainly from the ATLAS-CONF-2017-039 [63] search. This leads us to think that in the near future this model will be tested with a similar sensitivity to the other models. Currently the LEP limits are the strictest on this model, *cf.* Sec. IV.

#### E. Model IIIb

The relevant operator for Model IIIb is  $L_2 L_3 \bar{E}_3$ . This case is similar to Model IIIa, with the electrons in the final state of the stau decay replaced by muons, *cf.* Tab. I. The maximum branching ratio to muons is also 50%, as for the electrons in Model IIIa. The efficiency for muons is higher than for electrons and we expect a higher sensitivity. However, also in this case

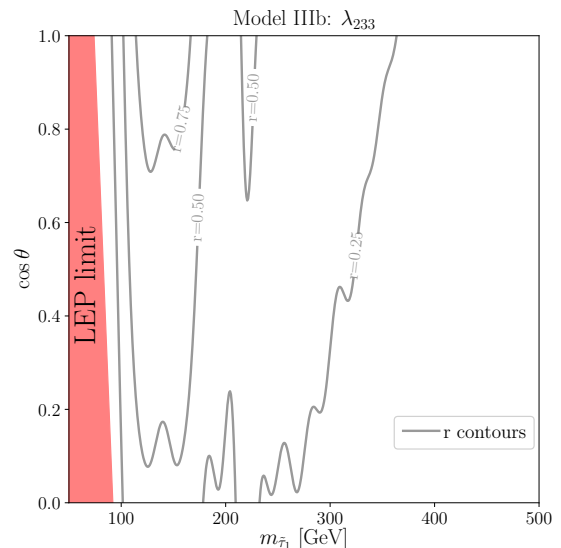


FIG. 11. As in Fig. 10 but for Model IIIb.

the searches implemented in **CheckMATE** are not sensitive enough to constrain Model IIIb. For that reason we depict in Fig. 11 iso-contours for  $r = 0.25, 0.50$  and  $0.75$ . The more promising region,  $r \geq 0.5$ , is as expected slightly larger than in Model IIIa, reaching lower values of  $\cos \theta_{\tilde{\tau}} \geq 0.1$ . We expect that future searches will be sensitive to this scenario. Again, currently the LEP limits are the strictest on this model, *cf.* Sec. IV.

## VII. CONCLUSIONS

We have examined the the pair production of super-symmetric staus followed by the direct RPV decay via  $L_i L_j \bar{E}_k$  operators at the LHC. We assume these decays comprise 100% of the branching ratios, corresponding to assuming the stau is the LSP, which is indeed the case for a large range of parameters in the RPV-CMSSM. To compare with data we have employed the program **CheckMATE**. We have demonstrated that current data from LHC set significant bounds on the lightest stau mass and the relevant stau mixing angle. The stau LSP decays via the  $LL\bar{E}$  into SM leptons. Therefore existing experimental searches for new physics in multileptonic channels can significantly constrain such scenarios. Current searches are able to put lower limits on the mass of the staus, with however a significant gap between the lower LEP limit and the onset of current LHC sensitivity. For the scenario where the stau can only decay into electrons and neutrinos ( $L_{1,2} L_3 \bar{E}_1$ ) the mass exclusion limit is set to  $m_{\tilde{\tau}_1} > 225$  (322) GeV for right-handed (left-handed) staus. If the staus decay only into muons and neutrinos ( $L_{1,2} L_3 \bar{E}_2$ ), the limits are  $m_{\tilde{\tau}_1} > 240$  (345) GeV for right-handed (left-handed) staus. When the decay into both electrons and muons is open ( $L_1 L_2 \bar{E}_3$ ), then the

searches are less efficient. In the case of pure left-handed staus the mass limit is  $m_{\tilde{\tau}_1} > 305$  GeV. However, in the case of pure right-handed staus the lower mass limit is  $m_{\tilde{\tau}_1} > 225$  GeV, with however a significant gap in sensitivity between 180 GeV and 205 GeV. And as in all cases there is a gap between the lower LEP limit and the onset of the LHC sensitivity. For a detailed stau mixing angle dependence of all above bounds see Figs. 7-9.

In the scenarios where the stau decays to tau leptons with at least 50% branching ratio ( $L_{1,2}L_3\bar{E}_3$ ), the current searches implemented in **CheckMATE** are not sensitive enough to set limits on the mass of the stau. We expect that in future runs of the LHC most of the parameter

space could be explored by new multilepton searches.

## ACKNOWLEDGEMENTS

We would like to thank Manuel Krauss for interesting discussions and collaboration in the initial phase of this project. HKD and VML acknowledge support of the BMBF-Verbundforschungsprojekt 05H18PDCA1. HKD thanks SCIPP at UCSC for kind hospitality, while part of this work was completed. VML acknowledges support by the Deutsche Forschungsgemeinschaft (DFG, German Research Foundation) under Germany's Excellence Strategy - EXC 2121 "Quantum Universe" - 390833306.

- 
- [1] H. P. Nilles, *Phys. Rept.* **110**, 1 (1984).  
 [2] S. P. Martin, , 1 (1997), [Adv. Ser. Direct. High Energy Phys.18,1(1998)], arXiv:hep-ph/9709356 [hep-ph].  
 [3] E. Gildener, *Phys. Rev.* **D14**, 1667 (1976).  
 [4] M. J. G. Veltman, *Acta Phys. Polon.* **B12**, 437 (1981).  
 [5] B. C. Allanach, A. Dedes, and H. K. Dreiner, *Phys. Rev.* **D60**, 056002 (1999), [Erratum: *Phys. Rev.*D86,039906(2012)], arXiv:hep-ph/9902251 [hep-ph].  
 [6] B. C. Allanach, A. Dedes, and H. K. Dreiner, *Phys. Rev.* **D69**, 115002 (2004), [Erratum: *Phys. Rev.*D72,079902(2005)], arXiv:hep-ph/0309196 [hep-ph].  
 [7] A. Yu. Smirnov and F. Vissani, *Phys. Lett.* **B380**, 317 (1996), arXiv:hep-ph/9601387 [hep-ph].  
 [8] G. R. Farrar and P. Fayet, *Phys. Lett.* **76B**, 575 (1978).  
 [9] J. R. Ellis, G. B. Gelmini, J. L. Lopez, D. V. Nanopoulos, and S. Sarkar, *Nucl. Phys.* **B373**, 399 (1992).  
 [10] H. Goldberg, *Phys. Rev. Lett.* **50**, 1419 (1983).  
 [11] L. E. Ibanez and G. G. Ross, *Phys. Lett.* **B260**, 291 (1991).  
 [12] H. K. Dreiner, C. Luhn, and M. Thormeier, *Phys. Rev.* **D73**, 075007 (2006), arXiv:hep-ph/0512163 [hep-ph].  
 [13] H. K. Dreiner, , 462 (1997), [Adv. Ser. Direct. High Energy Phys.21,565(2010)], arXiv:hep-ph/9707435 [hep-ph].  
 [14] R. Barbier *et al.*, *Phys. Rept.* **420**, 1 (2005), arXiv:hep-ph/0406039 [hep-ph].  
 [15] H. K. Dreiner, C. Luhn, H. Murayama, and M. Thormeier, *Nucl. Phys.* **B774**, 127 (2007), arXiv:hep-ph/0610026 [hep-ph].  
 [16] H. K. Dreiner, M. Hanussek, J.-S. Kim, and C. H. Kom, *Phys. Rev.* **D84**, 113005 (2011), arXiv:1106.4338 [hep-ph].  
 [17] H. K. Dreiner, M. Hanussek, and C. Luhn, *Phys. Rev.* **D86**, 055012 (2012), arXiv:1206.6305 [hep-ph].  
 [18] L. J. Hall and M. Suzuki, *Nucl. Phys.* **B231**, 419 (1984).  
 [19] R. Hempfling, *Nucl. Phys.* **B478**, 3 (1996), arXiv:hep-ph/9511288 [hep-ph].  
 [20] E. J. Chun and H. B. Kim, *Phys. Rev.* **D60**, 095006 (1999), arXiv:hep-ph/9906392 [hep-ph].  
 [21] K. Choi, E. J. Chun, and K. Hwang, *Phys. Rev.* **D64**, 033006 (2001), arXiv:hep-ph/0101026 [hep-ph].  
 [22] S. Colucci, H. K. Dreiner, and L. Ubaldi, *Phys. Rev.* **D99**, 015003 (2019), arXiv:1807.02530 [hep-ph].  
 [23] S. Colucci, H. K. Dreiner, F. Staub, and L. Ubaldi, *Phys. Lett.* **B750**, 107 (2015), arXiv:1507.06200 [hep-ph].  
 [24] H. K. Dreiner and G. G. Ross, *Nucl. Phys.* **B365**, 597 (1991).  
 [25] B. C. Allanach, M. A. Bernhardt, H. K. Dreiner, C. H. Kom, and P. Richardson, *Phys. Rev.* **D75**, 035002 (2007), arXiv:hep-ph/0609263 [hep-ph].  
 [26] D. Dercks, H. Dreiner, M. E. Krauss, T. Opferkuch, and A. Reinert, *Eur. Phys. J.* **C77**, 856 (2017), arXiv:1706.09418 [hep-ph].  
 [27] P. Bechtle *et al.*, *Proceedings, 2013 EPS Conference on High Energy Physics: Stockholm, Sweden, July 18-24, 2013*, *PoS EPS-HEP2013*, 313 (2013), arXiv:1310.3045 [hep-ph].  
 [28] P. Bechtle *et al.*, *Eur. Phys. J.* **C76**, 96 (2016), arXiv:1508.05951 [hep-ph].  
 [29] H. K. Dreiner and S. Grab, *Phys. Lett.* **B679**, 45 (2009), arXiv:0811.0200 [hep-ph].  
 [30] K. Desch, S. Fleischmann, P. Wienemann, H. K. Dreiner, and S. Grab, *Phys. Rev.* **D83**, 015013 (2011), arXiv:1008.1580 [hep-ph].  
 [31] G. Aad *et al.* (ATLAS), *JHEP* **12**, 124 (2012), arXiv:1210.4457 [hep-ex].  
 [32] M. Tanabashi *et al.* (Particle Data Group), *Phys. Rev.* **D98**, 030001 (2018).  
 [33] M. Drees, in *Current topics in physics. Proceedings, Inauguration Conference of the Asia-Pacific Center for Theoretical Physics (APCTP), Seoul, Korea, June 4-10, 1996. Vol. 1, 2* (1996) arXiv:hep-ph/9611409 [hep-ph].  
 [34] Y. Kao and T. Takeuchi, (2009), arXiv:0910.4980 [hep-ph].  
 [35] H. K. Dreiner, K. Nickel, F. Staub, and A. Vicente, *Phys. Rev.* **D86**, 015003 (2012), arXiv:1204.5925 [hep-ph].  
 [36] H. K. Dreiner, P. Richardson, and M. H. Seymour, *Phys. Rev.* **D63**, 055008 (2001), arXiv:hep-ph/0007228 [hep-ph].  
 [37] H. K. Dreiner, S. Grab, M. Krämer, and M. K. Trenkel, *Phys. Rev.* **D75**, 035003 (2007), arXiv:hep-ph/0611195 [hep-ph].  
 [38] H. K. Dreiner and T. Stefaniak, *Phys. Rev.* **D86**, 055010 (2012), arXiv:1201.5014 [hep-ph].  
 [39] M. Drees, H. Dreiner, D. Schmeier, J. Tattersall, and J. S. Kim, *Comput. Phys. Commun.* **187**, 227 (2015), arXiv:1312.2591 [hep-ph].

- [40] D. Dercks, N. Desai, J. S. Kim, K. Rolbiecki, J. Tattersall, and T. Weber, *Comput. Phys. Commun.* **221**, 383 (2017), [arXiv:1611.09856 \[hep-ph\]](#).
- [41] P. Richardson, *Simulations of R-parity violating SUSY models*, Ph.D. thesis, Oxford U. (2000), [arXiv:hep-ph/0101105 \[hep-ph\]](#).
- [42] H. K. Dreiner and G. G. Ross, *Nucl. Phys.* **B410**, 188 (1993), [arXiv:hep-ph/9207221 \[hep-ph\]](#).
- [43] B. C. Allanach, A. Dedes, and H. K. Dreiner, *Phys. Rev.* **D60**, 075014 (1999), [arXiv:hep-ph/9906209 \[hep-ph\]](#).
- [44] H. K. Dreiner, M. Hahnussek, and S. Grab, *Phys. Rev.* **D82**, 055027 (2010), [arXiv:1005.3309 \[hep-ph\]](#).
- [45] S. Bansal, A. Delgado, C. Kolda, and M. Quiros, (2019), [arXiv:1906.01063 \[hep-ph\]](#).
- [46] A. Heister *et al.* (ALEPH), *Eur. Phys. J.* **C31**, 1 (2003), [arXiv:hep-ex/0210014 \[hep-ex\]](#).
- [47] J. Abdallah *et al.* (DELPHI), *Eur. Phys. J.* **C36**, 1 (2004), [Erratum: *Eur. Phys. J.* C37,no.1,129(2004)], [arXiv:hep-ex/0406009 \[hep-ex\]](#).
- [48] P. Achard *et al.* (L3), *Phys. Lett.* **B524**, 65 (2002), [arXiv:hep-ex/0110057 \[hep-ex\]](#).
- [49] G. Abbiendi *et al.* (OPAL), *Eur. Phys. J.* **C33**, 149 (2004), [arXiv:hep-ex/0310054 \[hep-ex\]](#).
- [50] W. Porod, *Comput.Phys.Commun.* **153**, 275 (2003), [arXiv:hep-ph/0301101 \[hep-ph\]](#).
- [51] W. Porod and F. Staub, (2011), [arXiv:1104.1573 \[hep-ph\]](#).
- [52] F. Staub and W. Porod, *Eur. Phys. J.* **C77**, 338 (2017), [arXiv:1703.03267 \[hep-ph\]](#).
- [53] T. Sjöstrand, S. Ask, J. R. Christiansen, R. Corke, N. Desai, P. Ilten, S. Mrenna, S. Prestel, C. O. Rasmussen, and P. Z. Skands, *Comput. Phys. Commun.* **191**, 159 (2015), [arXiv:1410.3012 \[hep-ph\]](#).
- [54] R. D. Ball *et al.*, *Nucl. Phys.* **B867**, 244 (2013), [arXiv:1207.1303 \[hep-ph\]](#).
- [55] J. de Favereau, C. Delaere, P. Demin, A. Giammanco, V. Lemaitre, A. Mertens, and M. Selvaggi (DELPHES 3), *JHEP* **02**, 057 (2014), [arXiv:1307.6346 \[hep-ex\]](#).
- [56] M. Cacciari and G. P. Salam, *Phys. Lett.* **B641**, 57 (2006), [arXiv:hep-ph/0512210 \[hep-ph\]](#).
- [57] M. Cacciari, G. P. Salam, and G. Soyez, *Eur. Phys. J.* **C72**, 1896 (2012), [arXiv:1111.6097 \[hep-ph\]](#).
- [58] B. Fuks, M. Klasen, D. R. Lamprea, and M. Rothering, *JHEP* **01**, 168 (2014), [arXiv:1310.2621](#).
- [59] J. Fiaschi and M. Klasen, *JHEP* **03**, 094 (2018), [arXiv:1801.10357 \[hep-ph\]](#).
- [60] J. Fiaschi, M. Klasen, and M. Sunder, (2019), [arXiv:1911.02419 \[hep-ph\]](#).
- [61] G. Aad *et al.* (ATLAS), *JHEP* **06**, 124 (2014), [arXiv:1403.4853 \[hep-ex\]](#).
- [62] ATLAS-Collaboration, (2013), [ATLAS-CONF-2013-049](#).
- [63] ATLAS-Collaboration, (2017), [ATLAS-CONF-2017-039](#).